



Efficient Zr-doped FS–TiO₂/SiO₂ photocatalyst and its performance in acrylonitrile removal under simulated sunlight

Bandna Bharti¹ · Hanliang Li¹ · Dian Liu¹ · Hitanshu Kumar^{2,3} · Velu Manikandan⁴ · Xiaoxiong Zha¹ · Feng Ouyang^{1,5}

Received: 9 September 2020 / Accepted: 10 October 2020 / Published online: 23 October 2020
© Springer-Verlag GmbH Germany, part of Springer Nature 2020

Abstract

The aim of this research is to develop an efficient photocatalyst for the degradation of acrylonitrile under simulated sunlight. In this work, Zr-doped FS–TiO₂/SiO₂ photocatalyst was reported for the degradation of acrylonitrile. Sol–gel method were used for the preparation of Zr-doped FS–TiO₂/SiO₂ with the molar ratio of Ti:Zr varied from 1:0.07. The prepared photocatalyst was calcined at 450 °C for 2 h. The characteristics of Zr-doped FS–TiO₂/SiO₂ were examined by X-ray diffraction (XRD), ultraviolet–visible diffuse reflectance spectroscopy (UV–Vis DRS), scanning electron microscopy (SEM), transmission electron microscopy (TEM), Brunauer–Emmett–Teller (BET) and X-ray photoelectron spectroscopy (XPS). XRD results confirmed the presence of anatase phase of TiO₂, and it also reveals that the Zr doping did not change the crystal phase of TiO₂. The absorbance of Zr-doped FS–TiO₂/SiO₂ was significantly enhanced, as confirmed by the red shift in UV–Vis DRS spectra. Zr doping inhibits the recombination of electron–hole pairs and enhanced the photocatalytic activity. The UV–Vis DRS spectra show stronger absorption in Zr-doped FS–TiO₂/SiO₂ photocatalysts compared to FS–TiO₂/SiO₂. XPS analysis illustrated the presence of Zr⁴⁺, Ti³⁺, Ti⁴⁺, O²⁻ and OH groups in Zr-doped FS–TiO₂/SiO₂. Then, the photocatalytic activity of the prepared photocatalyst was tested for the photocatalytic degradation of acrylonitrile under simulated sunlight. Zr doping, together with F and S would enhance the surface area and charge separation, making it serve as a more effectual photocatalyst than TiO₂ and FS–TiO₂/SiO₂. The degradation ratio of acrylonitrile reached 79.2% within 6 min of simulated sunlight due to the doping effect of Zr into FS–TiO₂/SiO₂ photocatalyst. Zr doping could enhance the thermal stability of anatase phase of TiO₂ and improve its surface properties.

Keywords Doping · TiO₂ · Photocatalysis · Degradation · Acrylonitrile · Simulated sunlight

Hanliang Li has equal contribution as Bandna Bharti.

✉ Xiaoxiong Zha
zhaxx@hit.edu.cn

✉ Feng Ouyang
ouyangfh@hit.edu.cn; 329967681@qq.com

Bandna Bharti
bandna@hit.edu.cn; bandnathakurhp5@gmail.com

¹ School of Civil and Environmental Engineering, Harbin Institute of Technology, Shenzhen 518055, People's Republic of China

² Shenzhen Key Laboratory of Special Functional Materials and Shenzhen Engineering Laboratory for Advance Technology of Ceramics, College of Materials Science and Engineering, Shenzhen University, Shenzhen, People's Republic of China

³ Key Laboratory of Optoelectronic Devices and Systems of Ministry of Education and Guangdong Province, College of Optoelectronic Engineering, Shenzhen University, Shenzhen, People's Republic of China

⁴ Division of Biotechnology, College of Environmental and Bioresource Sciences, Chonbuk National University, Iksan 570-752, Korea

⁵ State Key Laboratory of Urban Water Resource and Environment, Harbin Institute of Technology, Harbin 150090, People's Republic of China

1 Introduction

The rapid progress in industrial society, biomass burning, transportation, urbanization and mining are becoming the major point of discussion in the ecological and environmental field. All these processes are responsible for the increased level of pollution in the environment which produces many negative effects on healthy lifestyle. To reduce environmental pollution, it is very requisite to find a sustainable strategy that maintains a clean and safe environment for living beings. In this respect, a variety of treatment methods are produced out of that photocatalysis is considered auspicious because it is low-cost, environmentally friendly as compared with other methods. TiO_2 , ZnO , SnO_2 , ZrO_2 , and CeO_2 are the common photocatalysts, among them photocatalysis with different combination structures of TiO_2 has been thoroughly studied [1–3]. TiO_2 has emerged as one of the most promising photo-induced catalysts and is repeatedly used to oxidize inorganic and organic compounds in water and air because of its long-term photo-stability and strong oxidative power [4]. Generally, numerous parameters, including morphology, crystallinity and specific surface area are responsible for the better photocatalytic activity of TiO_2 . However, poor conductivity and large bandgap of TiO_2 cause the difficulty in the transfer of electrons, which limits the credible applications of TiO_2 . Accordingly, some approaches have been employed to overcome the above-mentioned shortcoming to improve the properties of TiO_2 to increase its conductivity and reduce its bandgap [5]. Several ways can be applied to achieve this goal, such as doping with nonmetals and metals, surface modification by different treatments and coupling of TiO_2 with other semiconductor materials, etc. [6–9]. Previously, it has been reported that nonmetal doping could greatly enhance the absorption in the visible region. By contributing p-orbital, these nonmetals could easily substitute the O_2 atom from the lattice of TiO_2 [10–13]; because of this, the electronic properties of TiO_2 alters and results in the greater reaction rates for photocatalytic activity. Some investigations on fluoride doping has concerned significant attention, which led to the creation of surface oxygen vacancies and surface O^- species [14–16]. In our previous study, the higher photocatalytic activity of S–Bi co-doped F– $\text{TiO}_2/\text{SiO}_2$ was attributed to the increase in the number and strength of surface-active sites [17].

However, metal doping introduced some impurity levels between the valence and conduction band of TiO_2 which can significantly increase the speed of the photocatalytic process by reducing the electron–hole recombination [18]. Zirconium doping suppresses electron–hole recombination and increases the specific surface area that is most

important for the enhanced photocatalytic activity of TiO_2 [19]. Other studies reported the substitutional doping of Zr^{4+} ions into the lattice of TiO_2 . In addition, ZrTiO_4 species are formed in the presence of an excess of Zr^{4+} ions. The occurrence of both Zr^{4+} ions and surface NO_x species in a substitutional mode increases the total amount of charge carriers and enhances the absorption into the visible light region [20]. Furthermore, the addition of multiple dopants into the lattice of TiO_2 has become an active and promising method to improve the photocatalytic performance of TiO_2 as compared to singly and doubly doped system [21]. One such example is TiO_2 doped with iridium, carbon, nitrogen and it was found that multiple dopants reduce the band gap and shifts the absorption in the visible light region. These results give better photocatalytic H_2 evolution as compared to TiO_2 [22]. In our previous work, the photocatalytic activity was enhanced by F–S doping in the lattice of TiO_2 . But due to the poor stability of the photocatalyst, FS– $\text{TiO}_2/\text{SiO}_2$ needs further modification to increase the efficiency and stability of the photocatalyst. Therefore, in the present study, we report Zr-doped FS– $\text{TiO}_2/\text{SiO}_2$ photocatalyst synthesized by sol–gel method. The effect of Zr doping on the photocatalytic activity of FS– $\text{TiO}_2/\text{SiO}_2$ was investigated for the degradation of acrylonitrile under simulated sunlight. Here, acrylonitrile is selected as the target pollutant for photocatalysis.

Acrylonitrile (AN) is an important industrial material which is produced by the catalytic reaction of propylene with ammonia. It is widely used as a raw material for the production of synthetic rubber, plastics, acrylic fibers, resins, nitriles and acrylamide. Effluents discharged from the latex and chemical-manufacturing plants and acrylic industry wastewater are the main source of acrylonitrile [23]. Acrylonitrile is harmful and irritant to humans, who inhaled or directly contact with it. The symptoms for the inhalation of acrylonitrile are headache, nausea, irritation to throat and nose, vomiting and dizziness, whilst the long exposure of acrylonitrile causes cancer [24]. Therefore, to safe the water sources and environment, acrylonitrile wastewater must be treated before being discharged into the environment. In the previous literature, F- and S-doped TiO_2 has been studied extensively for its photocatalytic activity, whereas Zr-doped FS– $\text{TiO}_2/\text{SiO}_2$ photocatalyst has not been reported so far. Zr doping in FS– $\text{TiO}_2/\text{SiO}_2$ shows better photocatalytic activity.

2 Experimental section

2.1 Preparation of photocatalysts

Zr-doped FS– $\text{TiO}_2/\text{SiO}_2$ and FS– $\text{TiO}_2/\text{SiO}_2$ photocatalyst were prepared by sol–gel method. 5 mL butyl titanate was

dissolved in 13 mL of ethanol and this solution was stirred for 20 min at room temperature to form solution A. Further 0.45 mL of 40% HF, 21 mL of ethanol, 4.2 mL of glacial acetic acid, suitable amount of Zr (Ti:Zr ratio from 1:0.09) and 1.05 mL of deionized water were mixed together to form solution B. This solution was stirred ultrasonically for 5 min to form a clear solution. After that, solution B was added dropwise to solution A. After that, a suitable amount of silica was added (which can act as a capable carrier) in the above solution, which was continuously stirred for 2 h until the gel was formed. Here, silica gel can effectively disperse the titanium dioxide particles to inhibit their agglomeration, and increase the adsorption capacity due to its large specific surface area. The gel was aged for 10 h at room temperature, dried in an oven at 80 °C. After grinding the prepared gel, Zr-doped FS-TiO₂/SiO₂ was obtained by calcinating the gel powders in the air at different temperatures from 350 to 750 °C.

2.2 Photocatalytic activity test

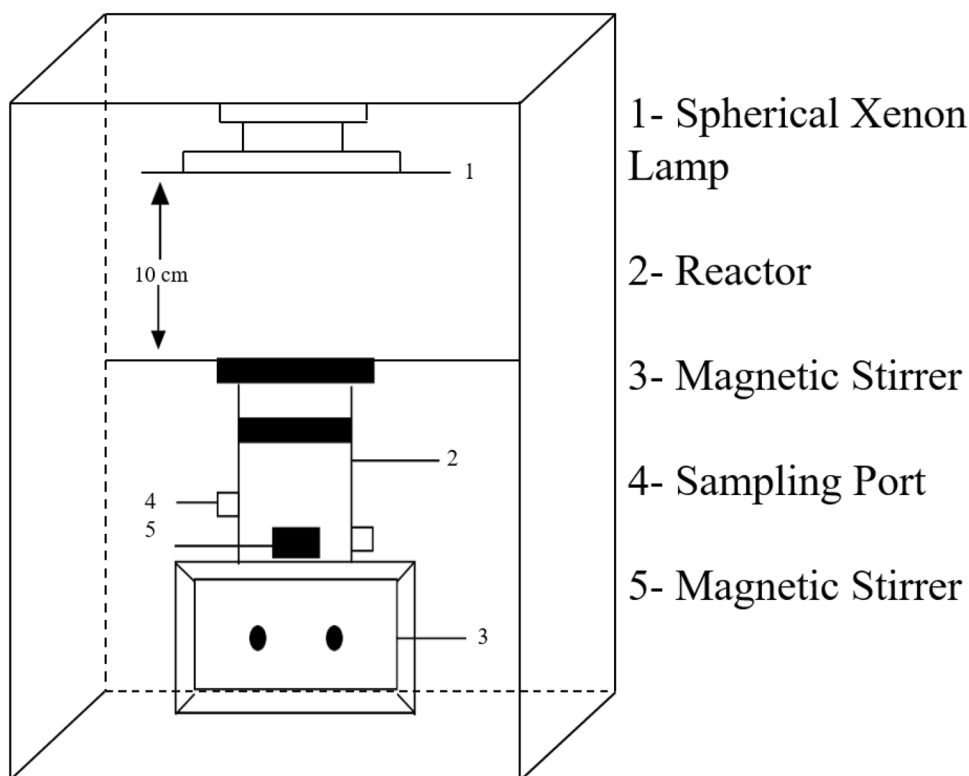
The photocatalytic reaction was performed in a quartz reactor as shown in Fig. 1. Acrylonitrile was used as the target pollutant to investigate the photocatalytic activity of the as-prepared photocatalyst under simulated sunlight. The concentration of the prepared acrylonitrile aqueous

solution was 10 mg/L. 180 mL of the solution was taken into a quartz reactor, and then 500 mg of the photocatalyst was weighed into it, after that the reactor was sealed with quartz glass to prevent the volatilization of acrylonitrile. Place the entire reactor in a special light-shielded reaction box, turn on the stirrer, stir evenly, close the reaction box, and make the reactor sealed. For the adsorption process, the photocatalyst was placed in the dark for 35 min to reach the equilibrium of adsorption and desorption, and then turn on the xenon lamp (350 W, Shenzhen An Hong Da Opto Technology Co., Ltd.). In the light process, a fan is used to cool the xenon lamp. At the same time, circulating cooling water is used to ensure that the reaction liquid in the reactor is at room temperature for the photocatalytic reaction. During the photocatalytic reaction, a sample solution of about 2 mL was withdrawn within the specific interval of time and the absorbance was measured using UV-Vis DRS spectroscopy. From the photocatalytic activity test, the percentage of acrylonitrile degraded by the prepared photocatalysts was determined from the following equation:

$$\text{Removal (\%)} = (C_0 - C_t) / C_0 \times 100,$$

where C_0 is the concentration of acrylonitrile (mg/L) after the adsorption and desorption equilibrium of the reaction system; C_t is acrylonitrile concentration (mg/L) in the reaction liquid after a certain period of photocatalytic reaction.

Fig. 1 The photocatalytic reactor designed for the degradation of acrylonitrile



2.3 Photocatalyst characterization

To find the crystal structure of Zr-doped FS-TiO₂/SiO₂ photocatalyst, X-ray diffraction (XRD) patterns were obtained on a Rigaku D/max 2500PC diffractometer with Cu K α radiation ($\lambda = 1.54056 \text{ \AA}$). A UV-Vis DRS spectroscopy was measured on Perkin Elmer Lambda 1050/950 UV spectrophotometer to find the light absorption of the photocatalyst. Transmission electron microscopy (TEM) (American FEI cooperation) F30 was used to analyze the physical properties of the photocatalysts. The samples were ultrasonically dispersed in ethanol which was supported on the copper grid. A scanning electron microscope (SEM) (HITACHISU8010) was used to study the morphology of the prepared photocatalyst.

To check the chemical states of each element, present in the photocatalyst, X-ray photoelectron spectroscopy (XPS) was performed on a Thermo ESCALAB 250XI instrument with Al K α X-ray source ($h\nu = 1486.6 \text{ eV}$). All binding energies were calibrated to the C1s peak of the instrument at 284.62 eV. The specific surface area of the prepared

photocatalyst was obtained using a Belsorp-mini nitrogen gas adsorption instrument (BET).

3 Results and discussion

3.1 Structural characterization of Zr-doped FS-TiO₂/SiO₂ photocatalyst

Figure 2 shows the XRD patterns of the prepared photocatalyst and their photocatalytic activity with an optimized condition (Ti:Zr 1:0.07 and calcination at 450 °C for 2 h). The XRD spectra of FS-TiO₂/SiO₂ and Zr-doped FS-TiO₂/SiO₂ are shown in Fig. 2a. It can be seen that the crystal phase of FS-TiO₂/SiO₂ and Zr-doped FS-TiO₂/SiO₂ were anatase phase which was confirmed by the presented peaks in XRD pattern. There was no prominent diffraction peak of Zr in the XRD of Zr-doped FS-TiO₂/SiO₂ photocatalyst because the concentration of Zr ions was below the detection limit of XRD and indicated the relatively uniform distribution of Zr. The crystallite size was calculated with the

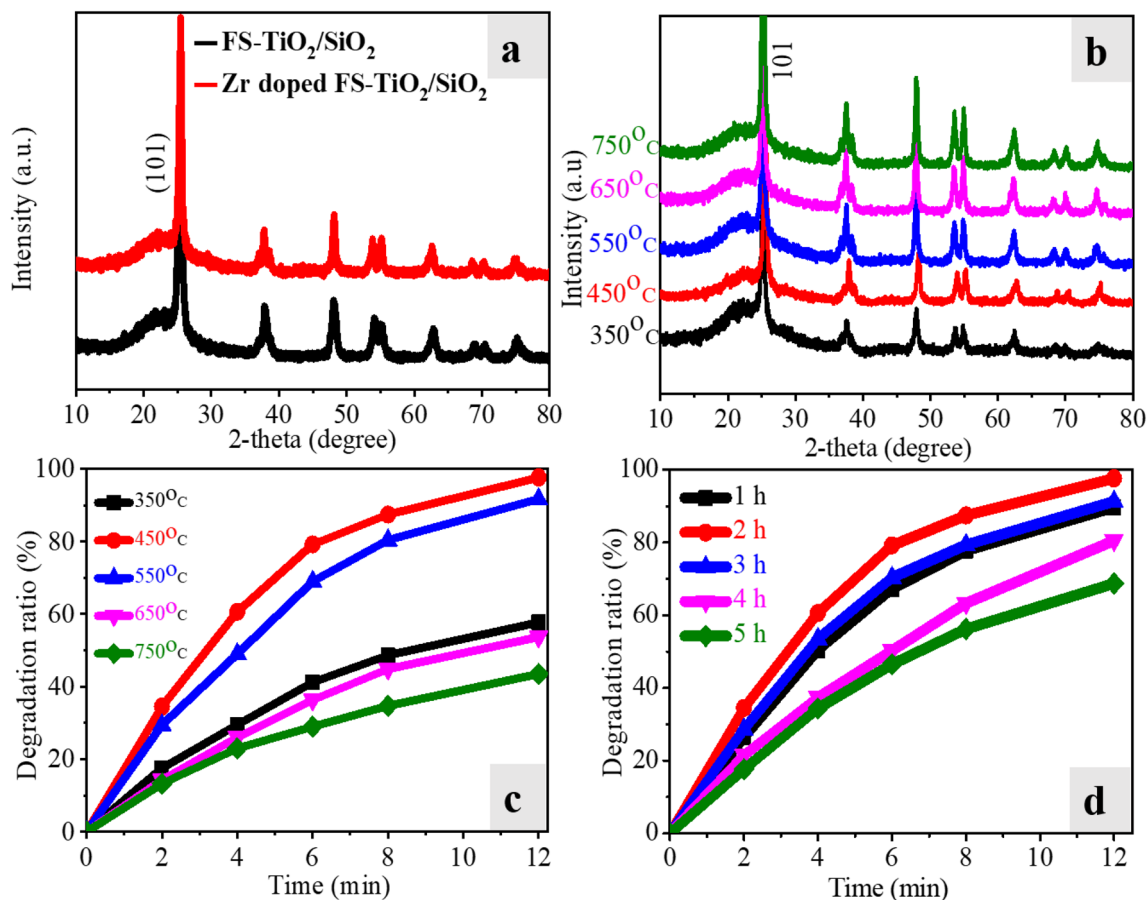


Fig. 2 a XRD patterns of FS-TiO₂/SiO₂ and Zr-doped FS-TiO₂/SiO₂ photocatalyst. b XRD patterns of Zr-doped FS-TiO₂/SiO₂ photocatalysts calcined at different temperature and c, d influence of calcination temperature and time on the activity of Zr-doped FS-TiO₂/SiO₂

help of Debye–Scherrer’s formula using the major crystal plane at (101) [25]. The crystallite size of FS–TiO₂/SiO₂ and Zr-doped FS–TiO₂/SiO₂ were 16.9 and 13.4 nm, respectively. It was found that the crystal phase for all the calcined samples corresponded to the anatase phase (Fig. 2b) [26]. Figure 2b clearly shows that no characteristic peaks of the rutile phase were formed in all the samples; it means doping with Zr does not allow the formation of the rutile phase even at a higher temperature. As the calcination temperature increased from 350 to 750 °C, the peaks became narrow which confirmed the better crystallinity of the prepared photocatalysts. Instead, with the increased calcination temperature, the anatase phase was maintained with relative peak intensities. This can be explained by the fact that Ti⁴⁺ is less electropositive than Zr⁴⁺. As a result of Zr doping, the electronic cloud in FS–TiO₂/SiO₂ will be more loosely held thus favoring the formation of the less dense anatase phase [26]. No characteristic peaks of Zr indicate the better dispersion of Zr in the prepared photocatalyst.

The effect of calcination temperature on the crystallite size is shown in Table 1 (green rows). It was found that the crystallite size and specific surface area were correlated with the calcination temperature. First, the specific surface area was increased when the temperature reached to 450 °C; after that, it decreased as the temperature increased from 450 to 750 °C. The higher calcination temperature can cause the photocatalyst to agglomerate the individual particles and thereby increasing the crystallite size and reducing the specific surface area. The prepared Zr-doped FS–TiO₂/SiO₂ photocatalyst was evaluated for the photocatalytic degradation of acrylonitrile under simulated sunlight, to investigate the effect of different calcination temperatures.

In Fig. 2c, the doping concentration of Ti:Zr was the same but the calcination temperature was increased from 350 to 750 °C. The degradation ratio of acrylonitrile was increased (79.2%) when the calcination temperature changed from 350 to 450 °C which results in the enhancement of crystallinity and the specific surface area of the prepared photocatalyst (Table 1). Further with the increase in the calcination temperature, there was a

gradual decrease in the degradation ratio which may be attributed to the agglomeration of the photocatalyst with the increase in the crystallite size.

Figure 2d illustrates the effect of calcination time on the photocatalytic degradation ratio of acrylonitrile. Here, we used the same optimized condition but varied the calcination time. It can be seen that as the calcination time increases, the photocatalytic degradation ratio of acrylonitrile first increases and then decreases. When the photocatalyst calcination time was 2 h, acrylonitrile had the highest removal rate, reaching 79.2%.

Therefore, the prepared photocatalyst has an optimized calcination temperature (450 °C) with optimized calcination time (2 h). As shown in Table 1 (blue rows), the specific surface area of the photocatalyst increases as the calcination time increases up to 2 h. When the calcination time was 2 h, the specific surface area of the photocatalyst had the highest value, which was consistent with the photocatalytic activity.

3.2 Morphological characterization of Zr-doped FS–TiO₂/SiO₂ photocatalyst

Figure 3a, d shows the SEM images of FS–TiO₂/SiO₂ and Zr-doped FS–TiO₂/SiO₂ photocatalyst, at a calcination temperature of 450 °C for 2 h. FS–TiO₂/SiO₂ photocatalyst exhibits large irregular particles, formed by the phenomenon of agglomeration (Fig. 3a). However, in case of Zr-doped FS–TiO₂/SiO₂, a microsphere structure with uniform size was formed. With Zr doping, the particle size was decreased, which may be attributed to the presence of Zr⁴⁺ ions that inhibit the grain growth by providing dissimilar boundaries [27]. TEM images of Zr-doped FS–TiO₂/SiO₂ photocatalyst at different locations are shown in Fig. 3b, e. Crystal lattice fringes present in the TEM images illustrate the sharp edge and high crystallinity of the prepared photocatalyst. In Fig. 3b, e, the lattice fringes corresponding to the anatase phase are observed. The lattice fringes having spacing of 0.254, 0.367 and 0.245 nm corresponding to (101) plane of TiO₂, (110) plane of ZrO₂ and (200) plane of Ti₂ZrO which was shown in enlarged images in Fig. 3c, f. SEM and TEM results of the prepared photocatalyst revealed that the addition of Zr ions increases the dispersion of the photocatalyst which results in the increased active site and specific surface area. The probable reason for the increased dispersion of the photocatalyst can be summarized as the decreased particles size, and the thermal stability of the anatase phase as well as the formation of defects on the surface of FS–TiO₂/SiO₂. The inter planer distancing and their corresponding planes shows that Zr is properly doped and these results have good agreement with XRD results.

Table 1 Crystallite size and specific surface area of Zr-doped FS–TiO₂/SiO₂ photocatalyst obtained at different calcination temperatures and time

Calcination temperature (°C)	350	450	550	650	750
Crystallite size (nm)	13.8	13.4	19.8	21.0	22.2
Specific surface area (m ² /g)	213.17	221.22	219.55	214.70	208.20
Calcination time (h)	1.0	2.0	3.0	4.0	5.0
Specific surface area (m ² /g)	220.88	221.22	216.91	214.03	211.87

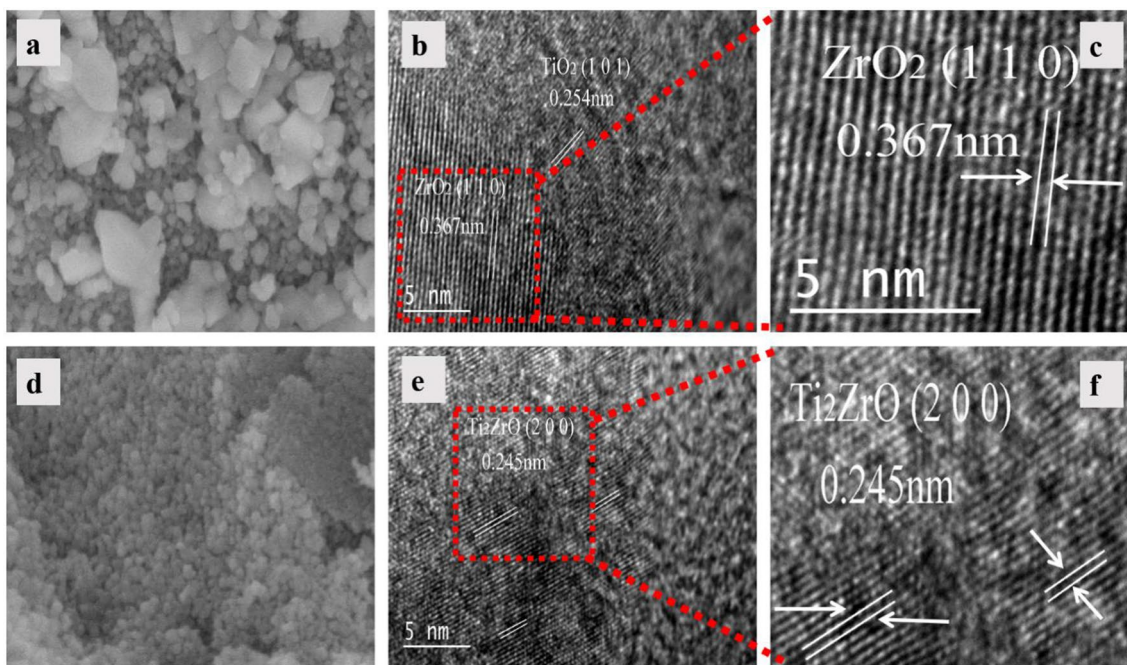


Fig. 3 a, d SEM images of FS–TiO₂/SiO₂ and Zr-doped FS–TiO₂/SiO₂ photocatalyst. b, e TEM image of Zr-doped FS–TiO₂/SiO₂ photocatalyst at different location. c, f Enlarge part of b and e

3.3 XPS characterization of Zr-doped FS–TiO₂/SiO₂ photocatalyst

XPS is used to determine the oxidation states of each

elements present in the prepared sample. XPS analysis was performed on Zr-doped FS–TiO₂/SiO₂ photocatalyst calcined at 450 °C. The XPS survey spectra and high-resolution spectra of Ti2*p*, O1*s*, F1*s*, S2*p* and Zr3*d* are

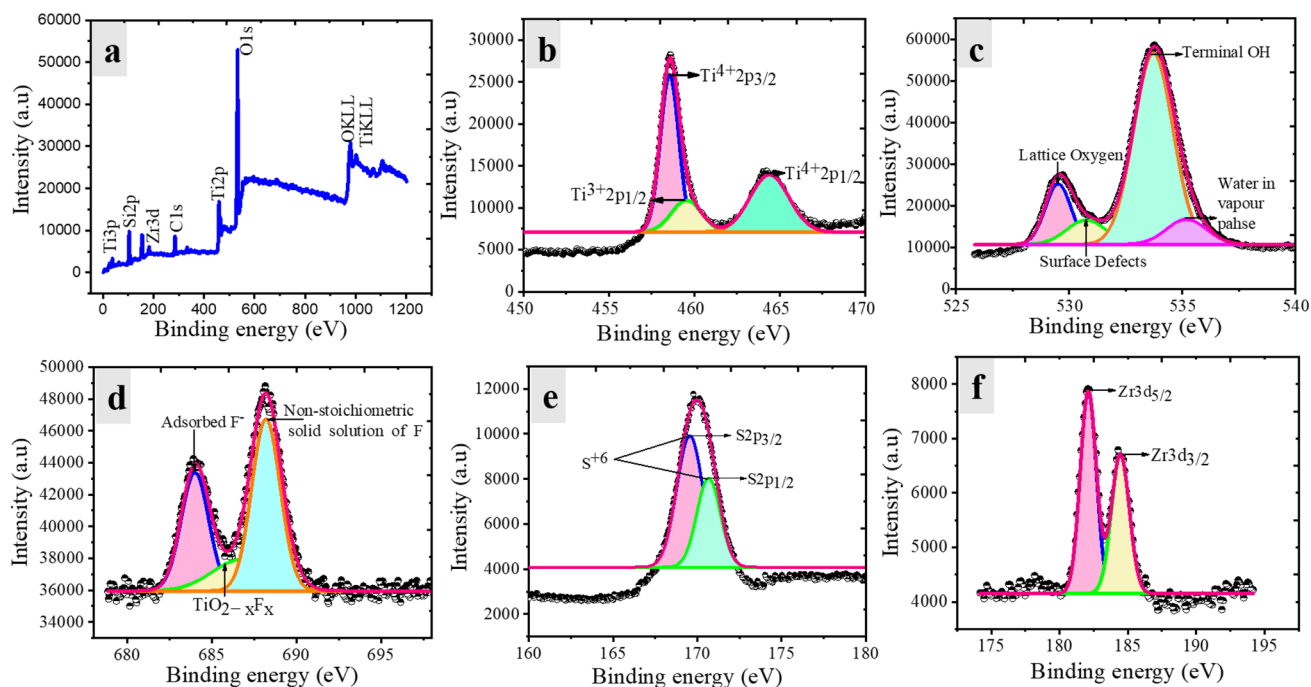


Fig. 4 a XPS survey spectra of Zr-doped FS–TiO₂/SiO₂, high-resolution XPS spectra of b Ti2*p*, c O1*s*, d F1*s*, e S2*p* and f Zr3*d*

illustrated in Fig. 4 for Zr-doped FS-TiO₂/SiO₂ photocatalyst. Figure 4a shows the XPS spectrum, which represents the existence of all element in the prepared photocatalyst. In this spectrum, the presence of carbon peaks was attributed to the XPS instruments itself [28]. The high-resolution XPS spectra for Ti2*p* are shown in Fig. 4b. Due to the spin-orbit coupling, Ti2*p* split into doublet at binding energy 458.6 and 464.4 eV, respectively. The peaks of Ti2*p* having binding energy at 458.6 and 464.4 eV correspond to the Ti2*p*_{3/2} and Ti2*p*_{1/2} chemical states. The difference in the binding energies (5.8 eV) of these peaks shows the presence of titanium in the +4-oxidation state [29]. However, a peak at binding energy 459.5 eV (Ti2*p*_{1/2}) also appeared in the spectra which corresponds to the titanium present in the +3-oxidation state [30]. These results indicate that Ti⁴⁺ ions occupy electrons from nearby oxygen vacancies and transform to Ti³⁺ ions.

Next, the O1*s* peak can be deconvoluted into four peaks as shown in Fig. 4c. The peak at binding energy 529.4 eV was attributed to the lattice oxygen present in TiO₂ [31]. Another three peaks at binding energy 530.7, 533.7 and 535.2 eV were corresponding to the surface defects/adsorbed hydroxyl groups [32], terminal OH group with an O-Ti⁴⁺ covalent bond [33] and water in vapor phase [34]. Figure 4d shows the high-resolution XPS spectra for F1*s*, deconvoluted into three peaks. The peak with binding energy 683.9 eV was assigned to the F⁻ anions, i.e., adsorbed on the surface of the photocatalyst (i.e., Ti-O-F or Ti-F bond, surface fluorination) [32]. The peaks at binding energy 686.5 and 688.1 eV were attributed to the substitutional F replacing O atoms resulting the structure of the type TiO_{2-x}F_x and a non-stoichiometric solid solution of F in TiO₂ [35]. Fluorine doping improves electron migration because of its higher electronegativity as compared to oxygen. These electrons were localized by Ti⁴⁺ to create Ti³⁺ trap states which can reduce the rate of charge recombination. The S2*p* XPS spectra of Zr-doped FS-TiO₂/SiO₂ are shown in Fig. 4e. After deconvolution, doublet of S2*p* peaks are observed. The peak at binding energy 169.5 eV (S2*p*_{3/2}) and a shoulder peak at binding energy 170.6 eV (S2*p*_{1/2}) indicate the presence of +6 oxidation state of S, when some of the Ti⁴⁺ ions in TiO₂ lattice were replaced by S⁶⁺ ions was consistent with previously reported work [36, 37]. Figure 4f shows the high-resolution XPS spectra of Zr3*d*. After fitting, two peaks with binding energy 182.1 and 184.4 eV were found in the prepared photocatalysts. The doublet in the Zr3*d* spectra (182.1 and 184.4 eV) could be attributed to Zr3*d*_{5/2} and Zr3*d*_{3/2} of substitutionally doped Zr⁴⁺ ions, since the peak of Zr3*d*_{5/2} lies between that of ZrO₂ (183.5 eV) and metallic Zr (179.0 eV) [38, 39] consistent with TEM results. Thus, it is confirmed from XPS analysis that Zr ions are incorporated into the TiO₂ lattice and replace some of the Ti⁴⁺ ions, because the electronegativity of Zr is higher than that of Ti.

It may be possible that some Zr-O-Ti links were formed from where the electrons transfer from Ti⁴⁺ to Zr⁴⁺ ions.

3.4 Optimization of photocatalysis parameters

UV-visible DRS spectra were performed to investigate the band structure of the prepared photocatalyst. Figure 5a shows the UV-Vis DRS spectra for pristine P25, FS-TiO₂/SiO₂ and Zr-doped FS-TiO₂/SiO₂. It can be found that, before the photocatalytic reaction, FS-TiO₂/SiO₂ and Zr-doped FS-TiO₂/SiO₂ photocatalysts has the strong absorption in the range of 200–380 nm, which was higher than that of commercial P25. However, in comparison between FS-TiO₂/SiO₂ and Zr-doped FS-TiO₂/SiO₂, the stronger absorption was shown by Zr-doped FS-TiO₂/SiO₂ photocatalyst, because Zr doping further enhances the absorption near the visible region. After the photocatalytic reaction, when the reaction was repeated five times, the FS-TiO₂/SiO₂ and Zr-doped FS-TiO₂/SiO₂ photocatalysts showed weaker absorption properties. This weaker absorption was responsible for the damage of photocatalyst during the photocatalytic process (data obtained from XPS analysis as shown in Table 2). The loss of light absorption was minute in the case of Zr-doped FS-TiO₂/SiO₂ photocatalyst, indicating that Zr modification improves the stability of the light absorption performance of the photocatalyst. The results show that Zr-doped FS-TiO₂/SiO₂ photocatalyst revealed higher activity after repeated reuse as compared to FS-TiO₂/SiO₂.

After Zr doping, it was found that the photocatalytic activity with different precursors of the same element (Zr) was not the same. Therefore, here, the precursors of Zr, which shows the best photocatalytic activity should be selected. Figure 5b shows the photocatalytic activity evaluation of FS-TiO₂/SiO₂ photocatalysts modified with different zirconium precursors. Three different precursors of Zr, i.e., zirconium oxychloride, zirconium nitrate, and zirconium oxynitrate were used to prepare Zr-doped FS-TiO₂/SiO₂ photocatalyst by sol-gel method with different ratio of Ti to Zr from 1:0.09 under optimized condition. A series of experiments are performed with acrylonitrile under the influence of simulated sunlight. The results show that the photocatalytic degradation rate of ZrOCl₂ after 6 min was 53.7%, which was lower than that of the FS-TiO₂/SiO₂ photocatalyst.

The photocatalytic degradation rate of Zr (NO₃)₃ after 6 min was 78.3%; however, the degradation rate of the pure FS-TiO₂/SiO₂ photocatalyst has no noticeable change as compared with the other two zirconium precursors. Zr (NO₃)₃ shows the best photocatalytic activity; therefore, in this study, Zr (NO₃)₃ was used as the precursor of Zr to prepare the corresponding photocatalyst. Figure 5c shows the evaluation of the photocatalytic activity of Zr-doped FS-TiO₂/SiO₂ photocatalysts with different doping ratios of

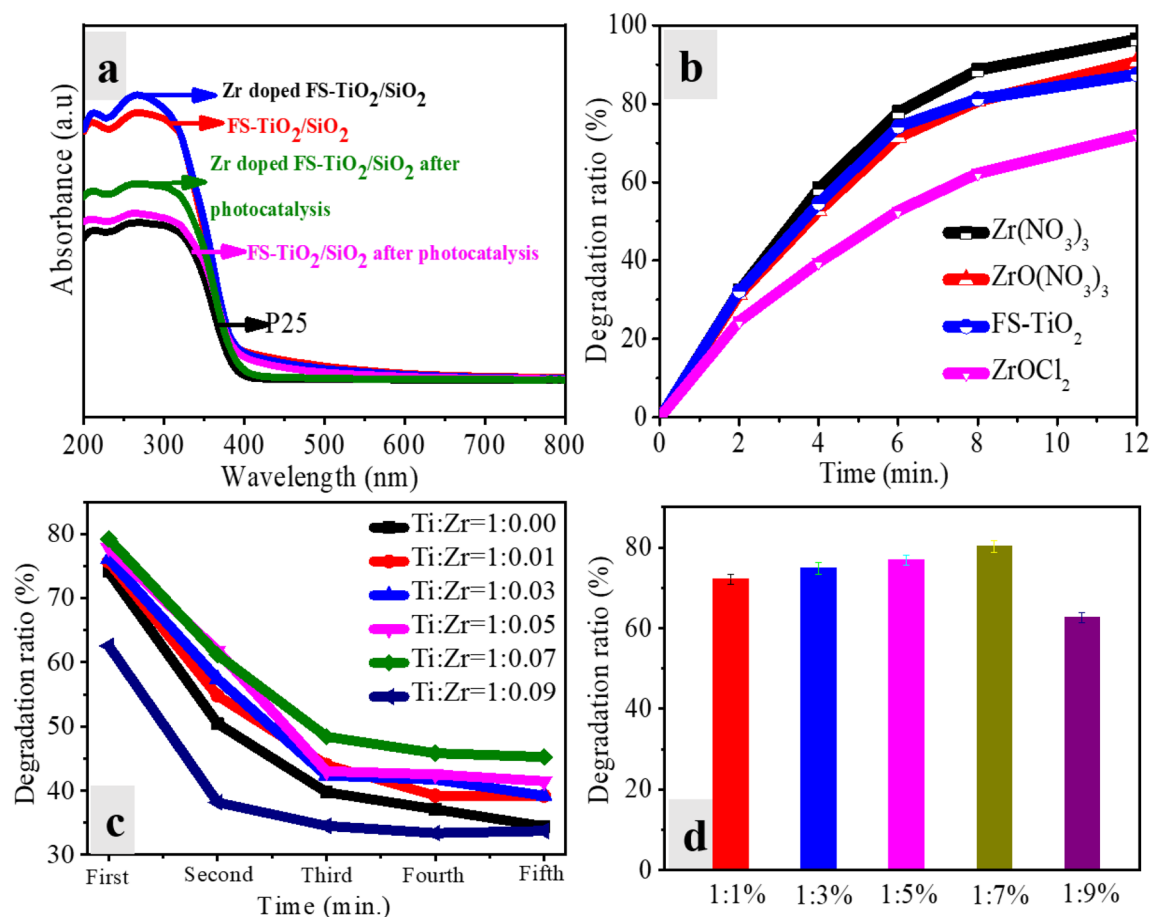


Fig. 5 **a** UV–Vis DRS spectra before and after the reaction of Zr-doped FS–TiO₂/SiO₂ photocatalyst. **b, c** Effect of Zr on the photocatalytic activity with different Zr precursor and molar ratio. **d** Effect of Zr ratio on the stability of prepared photocatalyst

Table 2 Percentage of each element present in FS–TiO₂/SiO₂ and Zr-doped FS–TiO₂/SiO₂ photocatalysts before and after the reaction

Name of the elements	FS–TiO ₂ /SiO ₂		Zr-doped FS–TiO ₂ /SiO ₂	
	Before reaction (%)	After reaction (%)	Before reaction (%)	After reaction (%)
C1s	41.65	42.38	52.42	57.08
Ti2p	37.92	52.35	21.16	35.62
S2p	1.73	2.24	2.49	2.52
F1s	18.70	3.03	23.93	4.78
Loss rate of F	83.8%		80.0%	

Zr under the optimized condition. The molar ratios of Ti:Zr varies from 1:0.0 to 1:0.09 and their corresponding photocatalytic degradation ratio for acrylonitrile within 6 min are 74.1, 75.7, 76.1, 77.8, 79.2, and 62.6%, respectively. It can be seen that the degradation efficiency of Zr-doped FS–TiO₂/SiO₂ photocatalyst was found to be increased with

the increase in the Zr doping ratio from 0.00 to 0.07 and decreased as the doping ratio was increased further. The maximum degradation efficiency (79.2%) to degrade acrylonitrile was observed with a doping ratio of 0.07. The reason for the decrease in the degradation efficiency with a higher doping ratio may be attributed to the formation of a new recombination center of photogenerated electrons on the surface of TiO₂. Appropriate doping ratio can improve the photocatalytic activity of Zr-doped FS–TiO₂/SiO₂ photocatalyst. As compared with FS–TiO₂/SiO₂, Zr-doped FS–TiO₂/SiO₂ photocatalyst shows higher photocatalytic activity. Hence, according to the experimental findings, the optimal doping ratio of Zr-doped FS–TiO₂/SiO₂ photocatalyst is 1:0.07.

To check the stability of prepared photocatalyst, the experiments were repeated five times. Figure 5d shows the Zr-doped FS–TiO₂/SiO₂ photocatalysts modified with different doping ratios of Zr after five repeated experiments. It was found that when the ratio of Ti to Zr was 1:0, the degradation ratio was 74.1% and after the fifth reaction, it decreased to 36.4%. Similarly, when the Zr doping increases,

the degradation ratio decreases after the completion of the fifth photocatalytic reaction. After the repeated experiment, the maximum photocatalytic degradation rate for acrylonitrile within 6 min was 45.25%, which was higher than that of FS-TiO₂/SiO₂ photocatalyst.

3.5 Photocatalytic mechanism

In general, the photocatalytic activity of a photocatalyst depends on the light absorption, specific surface area, recombination rate of photogenerated electron-hole pairs and crystallinity [40]. According to the above-mentioned results, the remarkably enhanced photocatalytic activity for the degradation of acrylonitrile by Zr-doped FS-TiO₂/SiO₂ photocatalyst could be explained by the schematic diagram as shown in Fig. 6. Zr-doped FS-TiO₂/SiO₂ photocatalyst provides additional ways of trapping holes and reducing the recombination of electro-hole pairs. During the photocatalytic reaction, the photocatalyst was irradiated with simulated sunlight. The electrons go directly from the valence band of TiO₂ to the doping level of Zr⁴⁺ ions or from the energy level of S to the conduction band of TiO₂. Meanwhile, the photogenerated holes in the valence band of TiO₂ move to the energy level of S and the photogenerated electron in the conduction band of TiO₂ moves to the doping level of Zr⁴⁺. On the surface of Zr-doped FS-TiO₂/SiO₂, the adsorbed oxygen captured the photogenerated electron present in the doping level of Zr⁴⁺ which act as electron trap centers resulting in the formation of O₂⁻ active species (O₂⁻) [41]. Moreover, the acrylonitrile adsorbed on the surface of Zr-doped FS-TiO₂/SiO₂ can be oxidized by the holes in the valence band of TiO₂ or in the energy level of S to produce hydroxyl radicals (OH). These active species are most important for the photocatalytic reaction which degrades the acrylonitrile further [42]. Afterward, Zr-doped FS-TiO₂/SiO₂ photocatalyst shows stronger absorbance in the visible region and enhanced the photocatalytic activity. This may be due to the substitutionally doped Zr⁴⁺ ions which form the

electron trap sites (as confirmed by XPS results) and energy level of S which separate the photogenerated electron and holes effectually.

On the other hand, the large specific surface area with a decreased particle size of FS-TiO₂/SiO₂ after Zr doping was also a significant point for the enhanced photocatalytic activity. Small particle size reduces the distance for the photogenerated electron towards the surface of the photocatalyst which results in the increased reaction sites on the surface. Furthermore, the enlarged specific surface area of the Zr-doped FS-TiO₂/SiO₂ in addition contributed to the increased photocatalytic activity as confirmed by BET results. In addition, it must be noted that, some of F⁻ ions are present on the surface of the photocatalyst. Fluorine doping improves the formation of surface acidic sites and oxygen vacancies, support the adsorption capacity of FS-TiO₂/SiO₂ photocatalyst and increase the separation of electron-hole pairs [43].

4 Conclusions

Zr-doped FS-TiO₂/SiO₂ photocatalyst was successfully synthesized by sol-gel method. The prepared photocatalyst has a large surface area and small crystallite size between 13 and 17 nm which has been achieved by optimized condition, i.e., calcination at 450 °C for 2 h with 1:0.07 ratio of Ti:Zr. The XRD results indicated the presence of anatase phase of TiO₂ and it was also confirmed from XRD analysis that metal doping did not change the crystal structure of TiO₂. In FS-TiO₂/SiO₂ photocatalyst, the F doping increases the surface acid sites and generates the Ti³⁺ state, whereas S doping enhances the absorption in the visible region. After Zr doping, further enhancement in the absorption due to the formation of electron trapping sites in Zr-doped FS-TiO₂/SiO₂ photocatalyst. The XPS results reveal the presence of F, S, Zr and Ti³⁺ states. After the repetition of fifth cycle, the photocatalytic activity of Zr-doped FS-TiO₂/SiO₂ photocatalyst

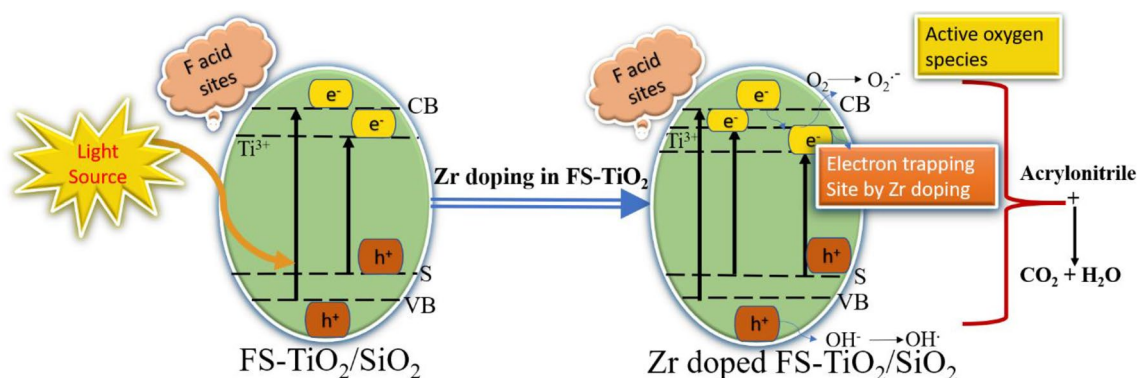


Fig. 6 Schematic diagram for the proposed photocatalytic mechanism of Zr-doped FS-TiO₂/SiO₂ photocatalyst

increased 8.9% for the degradation of acrylonitrile as compared to the FS–TiO₂/SiO₂ photocatalyst.

Acknowledgements This project was financially supported by the Foundation Science and Technology Innovation Committee of Shenzhen, P.R. China (no. JCYJ20150731104949798, no. ZDSYS201603301417588) and China Postdoctoral Science Foundation (FD29100012).

References

- W. Xie, R. Li, Q. Xu, *Sci. Rep.* **8**, 1–10 (2018)
- A. Mills, S. Le Hunte, *J. Photochem. Photobiol. A* **108**, 1–35 (1997)
- W. Fu, S. Ding, Y. Wang, L. Wu, D. Zhang, Z. Pan, R. Wang, Z. Zhang, S. Qiu, *Dalton Trans.* **43**, 16160–16163 (2014)
- V. Binias, D. Venieri, D. Kotzias, G. Kiriakidis, *J. Materiomics* **3**, 3–16 (2017)
- H.H. Do, D.L.T. Nguyen, X.C. Nguyen, T.H. Le, T.P. Nguyen, Q.T. Trinh, S.H. Ahn, D.V.N. Vo, S.Y. Kim, Q. Van Le, *Arab. J. Chem.* **13**, 3653–3671 (2020)
- Y.Q. Cao, X.R. Zhao, J. Chen, W. Zhang, M. Li, L. Zhu, X.J. Zhang, D. Wu, A.D. Li, *Sci. Rep.* **8**, 1–9 (2018)
- A. Šuligoj, I. Arčon, M. Mazaj, G. Dražić, D. Arčon, P. Cool, U.L. Štangar, N.N. Tušar, *J. Mater. Chem. A* **6**, 9882–9892 (2018)
- B. Bharti, S. Kumar, H.N. Lee, R. Kumar, *Sci. Rep.* **6**, 32355 (2016)
- H. Qiao, Z. Huang, S. Liu, Y. Tao, H. Zhou, M. Li, X. Qi, *J. Phys. Chem. C* **123**, 10949–10955 (2019)
- E.B. Simsek, *Appl. Catal. B* **200**, 309–322 (2017)
- W. Li, R. Liang, N.Y. Zhou, Z. Pan, *ACS Omega* **5**, 3808–3816 (2020)
- Y.J. Jin, J. Linghu, J. Chai, C.S. Chua, L.M. Wong, Y.P. Feng, M. Yang, S. Wang, *J. Phys. Chem. C* **122**, 16600–16606 (2018)
- W. Wang, Z. Wang, J. Liu, Z. Luo, S.L. Suib, P. He, G. Ding, Z. Zhang, L. Sun, *Sci. Rep.* **7**, 46610 (2017)
- M. Du, B. Qiu, Q. Zhu, M. Xing, J. Zhang, *Catal. Today* **327**, 340–346 (2019)
- C. Li, Z. Sun, R. Ma, Y. Xue, S. Zheng, *Microporous Mesoporous Mater.* **243**, 281–290 (2017)
- X. Yu, B. Jeon, Y.K. Kim, *ACS Catal.* **5**, 3316–3322 (2015)
- H. Li, L. Qiu, B. Bharti, F. Dai, M. Zhu, F. Ouyang, L. Lin, *Chemosphere* **249**, 126135 (2020)
- S.K. Md. Saad, A. Ali Umar, M.I. Ali Umar, M. Tomitori, M.Y. Abd. Rahman, M. Mat Salleh, M. Oyama, *ACS Omega* **3**, 2579–2587 (2018)
- J. Song, X. Wang, J. Yan, J. Yu, G. Sun, B. Ding, *Sci. Rep.* **7**, 1–12 (2017)
- P. Zhang, Y. Yu, E. Wang, J. Wang, J. Yao, Y. Cao, *ACS Appl. Mater. Interfaces* **6**, 4622–4629 (2014)
- A. Charanpahari, S.S. Umare, S.P. Gokhale, V. Sudarsan, B. Sreedhar, R. Sasikala, *Appl. Catal. A* **443**, 96–102 (2012)
- X.G. Zhao, L.Q. Huang, *Ceram. Int.* **43**, 3975–3980 (2017)
- P. Singh, A. Dhir, V.K. Sangal, *Desalination Water Treat* **55**, 1501–1508 (2015)
- D.S. Hill, J.K. O'Neill, R.J. Powell, D.W. Oliver, *J. Plast. Reconstr. Aesthet. Surg.* **65**, 911–916 (2012)
- Y.H. Lai, C.W. Chiu, J.G. Chen, C.C. Wang, J.J. Lin, K.F. Lin, K.C. Ho, *Sol. Energy Mater. Sol. Cells* **93**, 1860–1864 (2009)
- N. Venkatachalam, M. Palanichamy, B. Arabindoo, V. Murugesan, *J. Mol. Catal. A Chem.* **266**, 158–165 (2007)
- K.V. Bineesh, D.K. Kim, D.W. Park, *Nanoscale* **2**, 1222–1228 (2010)
- Y. Wang, T. Brezesinski, M. Antonietti, B. Smarsly, *ACS Nano* **3**, 1373–1378 (2009)
- T.V.L. Thejaswini, D. Prabhakaran, M.A. Maheswari, *J. Photochem. Photobiol. A* **344**, 212–222 (2017)
- L. Shen, Z. Xing, J. Zou, Z. Li, X. Wu, Y. Zhang, Q. Zhu, S. Yang, W. Zhou, *Sci. Rep.* **7**, 41978 (2017)
- N. Xu, L. Liu, X. Sun, X. Liu, D. Han, Y. Wang, R. Han, J. Kang, B. Yu, *Appl. Phys. Lett.* **92**, 232112 (2008)
- K. Subalakshmi, J. Senthilselvan, *Sol. Energy* **171**, 914–928 (2018)
- P. Krishnan, M. Liu, P.A. Itty, Z. Liu, V. Rheinheimer, M.H. Zhang, P.J. Monteiro, E.Y. Liya, *Sci. Rep.* **7**, 43298 (2017)
- G. Ketteler, P. Ashby, B.S. Mun, I. Ratera, H. Bluhm, B. Kasemo, M. Salmeron, *J. Phys. Condens. Matter.* **20**, 184024 (2008)
- J.C. Yu, J. Yu, W. Ho, Z. Jiang, L. Zhang, *Chem. Mater.* **14**, 3808–3816 (2002)
- T. Ohno, M. Akiyoshi, T. Umabayashi, K. Asai, T. Mitsui, M. Matsumura, *Appl. Catal. A* **265**, 115–121 (2004)
- C.D. Wagner, W.M. Riggs, L.E. Davis, J.F. Moulder, G.E. Muilenberg, *Eden Prairie, MN* **38** (1979)
- Z. Bastl, A.I. Senkevich, I. Spirovova, V. Vrtilkova, *Int. J. devoted to the development and application of techniques for the analysis of surfaces, interfaces and thin films* **34**, 477–480 (2002)
- I. Takano, S. Isobe, T.A. Sasaki, Y. Baba, *Appl. Surf. Sci.* **37**, 25–32 (1989)
- J. Xu, M. Chen, D. Fu, *Appl. Surf. Sci.* **257**, 7381–7386 (2011)
- M.R. Hoffmann, S.T. Martin, W. Choi, D.W. Bahnemann, *Chem. Rev.* **95**, 69–96 (1995)
- Y. Zhang, H. Xu, Y. Xu, H. Zhang, Y. Wang, *J. Photochem. Photobiol. A* **170**, 279–285 (2005)
- D. Li, N. Ohashi, S. Hishita, T. Kolodiazhnyi, H. Haneda, *J. Solid State Chem.* **178**, 3293–3302 (2005)

Publisher's Note Springer Nature remains neutral with regard to jurisdictional claims in published maps and institutional affiliations.